Elastic electron backscattering from surfaces with overlayers

A. Jablonski
Institute of Physical Chemistry, Polish Academy of Sciences, ul. Kasprzaka 44/52, 01-224 Warszawa, Poland

H. S. Hansen, C. Jansson, and S. Tougaard
Fysisk Institut, Odense Universitet, DK-5230 Odense M, Denmark
(Received 13 August 1991)

The most pronounced effects of elastic scattering in solids are observed in electron backscattering experiments, which, as a result, offer the possibility to test the completeness of the theoretical models of electron transport. For this purpose, elastic backscattering from the Au/Ni(111) system was studied in the present work. Since the total-elastic-scattering cross section for Au is considerably larger than that for Ni, one would expect from simple arguments that the observed elastic peak intensities increase as the Au overlayer thickness is increased. However, a considerable intensity decrease (by a factor of up to 5) with increasing overlayer thickness is observed at energies up to at least 500 eV. This unexpected behavior can be explained within the proposed theory as due to a particular arrangement of differential-scattering cross sections within the experimental geometry used. At higher energies the backscattered intensities increase, in agreement with expectations. In all cases, the predicted intensities compare very well with experimental observations. The low-energy-electron-diffraction pattern for polycrystalline gold shows a characteristic dark ring whose origin can be ascribed to the complex structure of the differential-elastic-scattering cross section of gold. The decreased elastic-backscattering probability within the dark ring is responsible for the unusual behavior of intensities observed in the overlayer experiments. The position of the dark ring is well explained by the proposed Monte Carlo algorithm.

I. INTRODUCTION

Recent developments in surface-sensitive electron spectroscopies have stimulated interest in the phenomenon of elastic backscattering. It has been demonstrated that elastic collisions of photoelectrons and Auger electrons[1–3] must be accounted for in the formalism of quantitative analysis. The validity of the corresponding theory cannot be readily verified since elastic-scattering effects in electron spectroscopies are difficult to visualize directly. However, the presence of the elastic peak in the energy spectra is a most convincing proof that elastic collisions do occur in the solid, and the theories of electron transport can be easily compared with elastic-backscattering experiments. Comparison is facilitated by the fact that elastic-backscattering effects are particularly pronounced at energies of 50–2000 eV,[4] i.e., in the range of energies of Auger electrons and photoelectrons. Furthermore, the phenomenon of elastic backscattering from surfaces is the basis for the experimental method providing the values of the inelastic mean free path of electrons.[5] For obvious reasons this method requires an accurate theoretical description of elastic backscattering.

It has been found that the Monte Carlo model involving an approximation of the electron trajectory by the Poisson stochastic process and the description of elastic-scattering events by the partial-wave-expansion method very well describe elastic electron backscattering from elemental solids.[6,7] In that case the theory almost reproduces the characteristics of backscattered electrons, i.e., the angular distribution and energy dependence of the monitored intensity. Good agreement with experimental observations is observed for medium-[6] and high[7]-atomic-number elements. In the latter case the theory compares well with experiment, despite the complicated structure of the angular distribution of backscattered electrons.

In the present work the theory of elastic backscattering is extended to more complicated systems, i.e., systems with overlayers. Experimental measurements and calculations are made for the high-atomic-number element deposited on the medium-atomic-number element, Au on Ni, since these two elements exhibit profoundly different scattering properties.

II. EXPERIMENT

Experiments were performed under UHV conditions (base pressure better than 10^{-10} torr) in a VG system equipped with x-ray photoemission spectroscopy (XPS) low-energy electron diffraction (LEED), and reflection electron-energy-loss spectroscopy (REELS). The electron energy analyzer (VG CLAM), of a concentric hemispherical type, was operated in the constant-resolution mode.[8] The Ni(111) crystal was mounted and cleaned in UHV as described elsewhere.[9] During elastic-backscattering measurements using the REELS facility, the analyzer axis was normal to the surface, while the angle between the incident electron beam and surface normal was 25°. High-purity gold was evaporated from a hot tungsten filament onto the Ni(111) surface at room temperature in successive steps with coverages varying from about 1 to 40 monolayers of gold. The thickness was monitored by

a quartz-crystal microbalance[9] and by the quantitative inelastic background analysis of the XPS spectra.[9,10] The absolute thicknesses thus obtained were in agreement to within 10–20%.[9,10] Only diffuse LEED pictures are observed from the Au/Ni(111) sample, thus indicating a gold overlayer growing with a low structural order.

The elastic peaks for the Au/Ni(111) sample were measured under fixed experimental conditions at energies $E_0=300$, 500, 1000, and 2000 eV for each Au overlayer thickness. The analyzer was operated at 20 eV pass energy. To avoid the effects of instabilities in the primary electron current, the elastic peak intensities for the Au/Ni(111) system, I_E, were measured with respect to the reference sample, which was the mechanically polished polycrystalline Au sample, carefully cleaned in UHV. The reproducibility of the ratio between the elastic peak areas for the Au/Ni(111) sample and reference Au sample, I_E/I_E^{ref}, was better than 5% for all measurements.

III. THEORY

A. Elastic-scattering cross sections

The theoretical model, successfully applied to elastic backscattering from elements,[6,7] requires knowledge of accurate elastic-scattering cross sections corresponding to the scattering centers in solids. The energy range of interest of surface-sensitive electron spectroscopies varies from about 100 to 2000 eV. In this energy range one encounters computational difficulties in calculations of the elastic-scattering cross sections. These energies are too low for the reliable application of the screened Rutherford cross section[11,12] or first-order Born approximation.[6] Both approximations do not predict the involved structure of the distribution of scattering angles. Thus the accurate solution of the scattering problem at considered energies is necessary, i.e., application of the partial-wave-expansion method. The nonrelativistic differential-elastic-scattering cross section is defined then by the well-known expression[13]

$$\frac{d\sigma}{d\Omega}=|f(\theta)|^2 , \tag{1a}$$

where θ is the scattering angle and $f(\theta)$ is the scattering amplitude, defined by

$$f(\theta)=\frac{1}{2iK}\sum_{l=0}^{\infty}(2l+1)[\exp(2i\delta_l)-1]P_l(\cos\theta) . \tag{1b}$$

In the above formula K denotes the length of the wave vector, δ_l denotes the lth phase shift, and $P_l(\cos\theta)$ is the Legendre polynomial of lth degree. On integration of Eq. (1a), we obtain the total-elastic-scattering cross section

$$\sigma_t=2\pi\int_0^{\pi}|f(\theta)|^2\sin\theta\, d\theta = \frac{4\pi}{K^2}\sum_{l=0}^{\infty}(2l+1)\sin^2\delta_l . \tag{2}$$

Convergence of the series (1b) or (2) depends on the sequence of the phase shifts. At low energies only a few phase shifts are sufficient to ensure good accuracy of the scattering amplitude and the total-elastic-scattering cross section.[14] However, in the energy range of the surface-sensitive electron spectroscopies, particularly at energies exceeding 1000 eV, the convergence rapidly deteriorates. The necessary number of phase shifts may reach 70–80. Obviously, an efficient method of determining the phase shifts should be applied in such a case. In the present work the method proposed by Calogero[15] was used. This method is briefly outlined below.

The radial Schrödinger equation can be transformed to the first-order differential equation

$$\delta_l'(r)=-\frac{1}{K}\frac{2m}{\hbar^2}V(r) \times[\hat{j}_l(Kr)\cos\delta_l(r)-\hat{n}_l(Kr)\sin\delta_l(r)]^2 , \tag{3}$$

where $V(r)$ is the scattering potential, $\hat{j}_l(x)$ and $\hat{n}_l(x)$ are the linearly independent solutions of the Riccati-Bessel differential equation, and other symbols have the usual meaning. The phase function $\delta_l(r)$ satisfying the initial condition

$$\delta_l(0)=0$$

approaches asymptotically the lth phase shift:

$$\lim_{r\to\infty}\delta_l(r)=\delta_l . \tag{4}$$

Equations (3) and (4) can be used effectively for calculating the phase shifts.[6]

Calogero also proposed an alternative approach based on the related first-order differential equation (Ref. 15, Chap. 13). On suitable substitution, Eq. (3) can be transformed to the form

$$\gamma_l'(r)=-\frac{1}{K}\left[\frac{l(l+1)}{r^2}+\frac{2m}{\hbar^2}V(r)\right]\sin^2[\gamma_l(r)+Kr] , \tag{5}$$

with the initial conditions

$$\gamma_l(0)=0 \quad\text{and}\quad \gamma_l'(0)=-Kl/(l+1) .$$

In that case the phase shifts are calculated from

$$\tan\delta_l=\lim_{r\to\infty}\frac{\cos[\gamma_l(r)+Kr]\hat{j}_l(Kr)-\sin[\gamma_l(r)+Kr]\hat{j}_l'(Kr)}{\cos[\gamma_l(r)+Kr]\hat{n}_l(Kr)-\sin[\gamma_l(r)+Kr]\hat{n}_l'(Kr)} .$$

Both first-order differential equations [Eqs. (3) and (5)] can be used in calculations of the phase shifts. Details of the corresponding algorithms are available elsewhere.[6,7] Integration of Eq. (3) has the advantage of providing the absolute values of the phase shifts. On the other hand, calculations involving integration of Eq. (5) lead to the values of $\delta_l \mathrm{mod}\pi$; however, the corresponding algorithm is noticeably faster. This is due to the fact that the Riccati-Bessel functions are not present in the right-hand side of Eq. (5) and do not have to be determined at each step of the integration. Calculations of these functions with sufficient accuracy usually require a considerable amount of computations. Both methods of calculating the phase shifts were used in the present work and were found to provide identical results. As in earlier reports,[6,7] the scattering potentials of the solid were approximated by the corresponding Thomas-Fermi-Dirac (TFD) potentials for neutral atoms.[16,17]

B. Electron transport

The electron trajectories in the overlayer-substrate systems were simulated by the Monte Carlo method. In the usual simulation schemes, the trajectories are assumed to be composed of linear steps between elastic-scattering events. Furthermore, the trajectories are approximated by the Poisson stochastic process. In that case the linear-step lengths Δx follow the exponential distribution[3]

$$f(\Delta x)=(1/\lambda_e)\exp(-\Delta x/\lambda_e) ,$$

where λ_e is the elastic mean free path, i.e., the average length of the linear steps. It is usually calculated from[18–20]

$$\lambda_e=(N\sigma_t)^{-1} ,$$

where N is the number of atoms in units of volume.

The above formalism applies to uniform solids. In the case of systems with overlayers, the distribution of the step lengths is more involved. Let us consider the system consisting of two materials A and B, separated by a sharp interface. Suppose that the considered electron is in material A at distance D from the interface and is moving toward the interface. Furthermore, we assume that an electron does not change direction on passing the interface. It can be shown that the distribution of linear-step lengths for the considered case is[20]

$$f(\Delta x)=\begin{cases}(1/\lambda_e^{(A)})\exp(-\Delta x/\lambda_e^{(A)}) & \text{if } 0<\Delta x<D ,\\ \dfrac{\exp(-D/\lambda_e^{(A)})}{\exp(-D/\lambda_e^{(B)})}(1/\lambda_e^{(B)})\exp(-\Delta x/\lambda_e^{(B)}) & \text{if } \Delta x>D ,\end{cases}$$

where $\lambda_e^{(A)}$ and $\lambda_e^{(B)}$ are the elastic mean free paths of electrons in materials A and B, respectively. The above distribution can be easily simulated. Corresponding calculations consist of two states. At first we generate the step length Δx_A in uniform material A. In the second stage we apply the rule

$$\Delta x=\begin{cases}\Delta x_A & \text{if } \Delta x_A<D ,\\ D+(\Delta x_A-D)(\lambda_e^{(B)}/\lambda_e^{(A)}) & \text{if } \Delta x_A>D .\end{cases}$$

The contribution to the backscattered current due to the ith electron trajectory is calculated from

$$\Delta I_i=\begin{cases}\exp\left[-\left[\dfrac{x_i^{(A)}}{\lambda^{(A)}}+\dfrac{x_i^{(B)}}{\lambda^{(B)}}\right]\right] & \text{when the electron left the solid within the considered solid angle ,}\\ 0 & \text{otherwise ,}\end{cases}$$

where $x_i^{(A)}$ and $x_i^{(B)}$ are the total trajectory lengths traversed in materials A and B, respectively, and $\lambda^{(A)}$ and $\lambda^{(B)}$ are the corresponding inelastic mean free paths. Eventually, the backscattered intensity is estimated from

$$I=\frac{1}{n}\sum_{i=1}^{n}\Delta I_i ,$$

where n is the total number of trajectories. The elastic-backscattering probabilities are relatively low.[4] Thus a considerable number of the trajectories must be generated to obtain reasonable accuracy of the estimated intensity I. In the present work, because of a rather limited solid acceptance angle, it was necessary to generate 2×10^6 trajectories for each energy and each overlayer thickness to obtain the accuracy of 1–3 %.

IV. RESULTS

One can expect that the elastic-backscattering properties of a solid are associated with the elastic-scattering cross sections due to the constituents of the solid. The total-elastic-scattering cross sections for different elements were calculated by a number of authors. Salvat, Mayol, and Martinez[14] compared the total-elastic-scattering cross section calculated for argon and mercury in the energy range 100–5000 eV using different theoretical approaches. Similar calculations made for aluminum

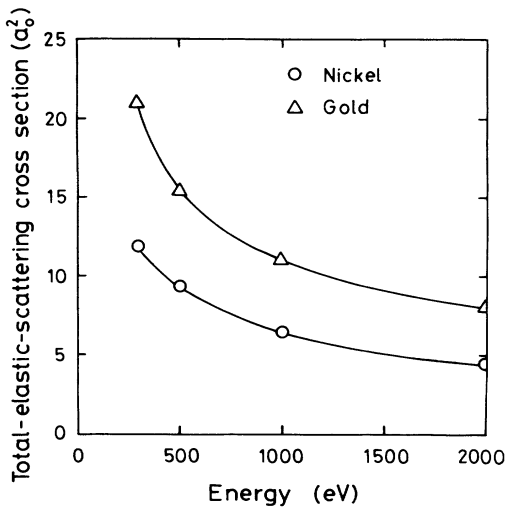

FIG. 1. Energy dependence of the total-elastic-scattering cross section calculated within nonrelativistic partial-wave-expansion method. Circles, nickel; triangles, gold.

and gold were published by Liljequist *et al.*[19] Ichimura and Shimizu[21] performed systematic calculations of the total-elastic-scattering cross sections for elements with atomic number ranging from 5 to 79 and energies up to 10 keV. Three conclusions result from all the above calculations.

(1) The total-elastic-scattering cross section increases monotonically with decreasing energy. The increase of σ_t is particularly pronounced in the range of low energies.

(2) The difference between two total-elastic-scattering cross sections for two elements also increases with decreasing energy.

(3) The total-elastic-scattering cross section at a given energy increases monotonically with the increase of the atomic number.

The energy dependence of the total-elastic-scattering cross sections calculated in the present work for nickel and gold are shown in Fig. 1. As one can see, the behavior of these plots is in agreement with observations of other authors. Thus one would expect that the deposition of gold on nickel should increase the elastic-

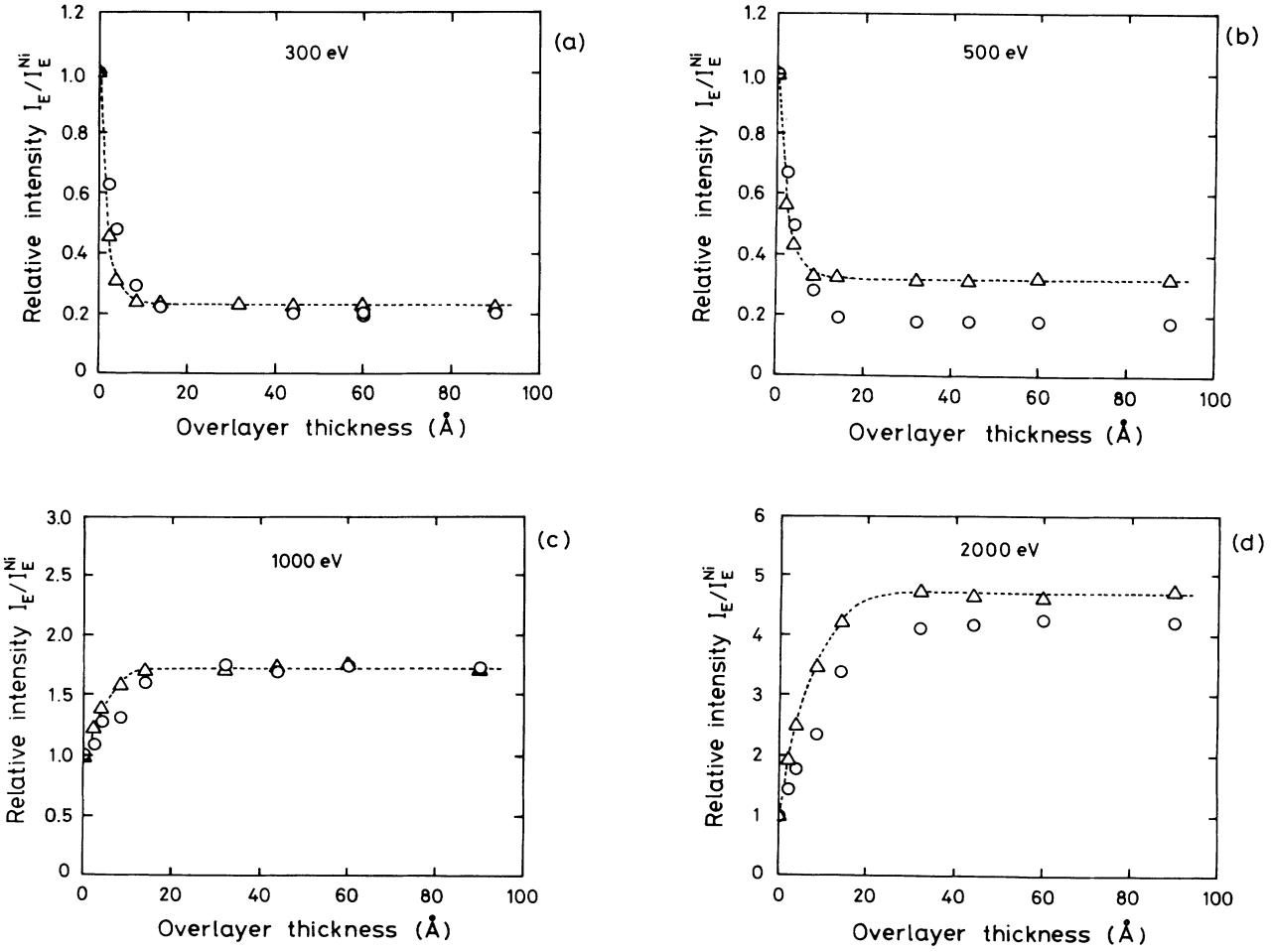

FIG. 2. Comparison of the experimental and theoretical overlayer thickness dependences of the ratio of elastic-backscattering intensities from a Au overlayer on nickel and from a nickel substrate, I_E/I_E^{Ni}. Circles, experiment; triangles and dashed line; Monte Carlo calculations. (a) 300 eV, (b) 500 eV, (c) 1000 eV, and (d) 2000 eV.

backscattering intensity, as a result of the considerably larger elastic-scattering cross section of Au, and this effect should be particularly pronounced at low energies. If the backscattered intensity can be described quantitatively by a reliable theory, a very simple and convenient method can be proposed for measurement of the overlayer thickness. However, the experimental intensities measured in the present work for the gold-on-nickel system were in dramatic disagreement with the above expectations. The experimental intensities normalized with respect to the uncovered Ni substrate, I_E/I_E^{Ni}, are listed in Table I. A considerable decrease of the elastic peak intensity with growing overlayer thickness was observed at the lowest energies, i.e., 300 and 500 eV. At higher primary energies the elastic peak intensity increases with the gold overlayer thickness, as expected. However, a more pronounced increase occurs at 2000 eV rather than at 1000 eV, which again is in contradiction with qualitative

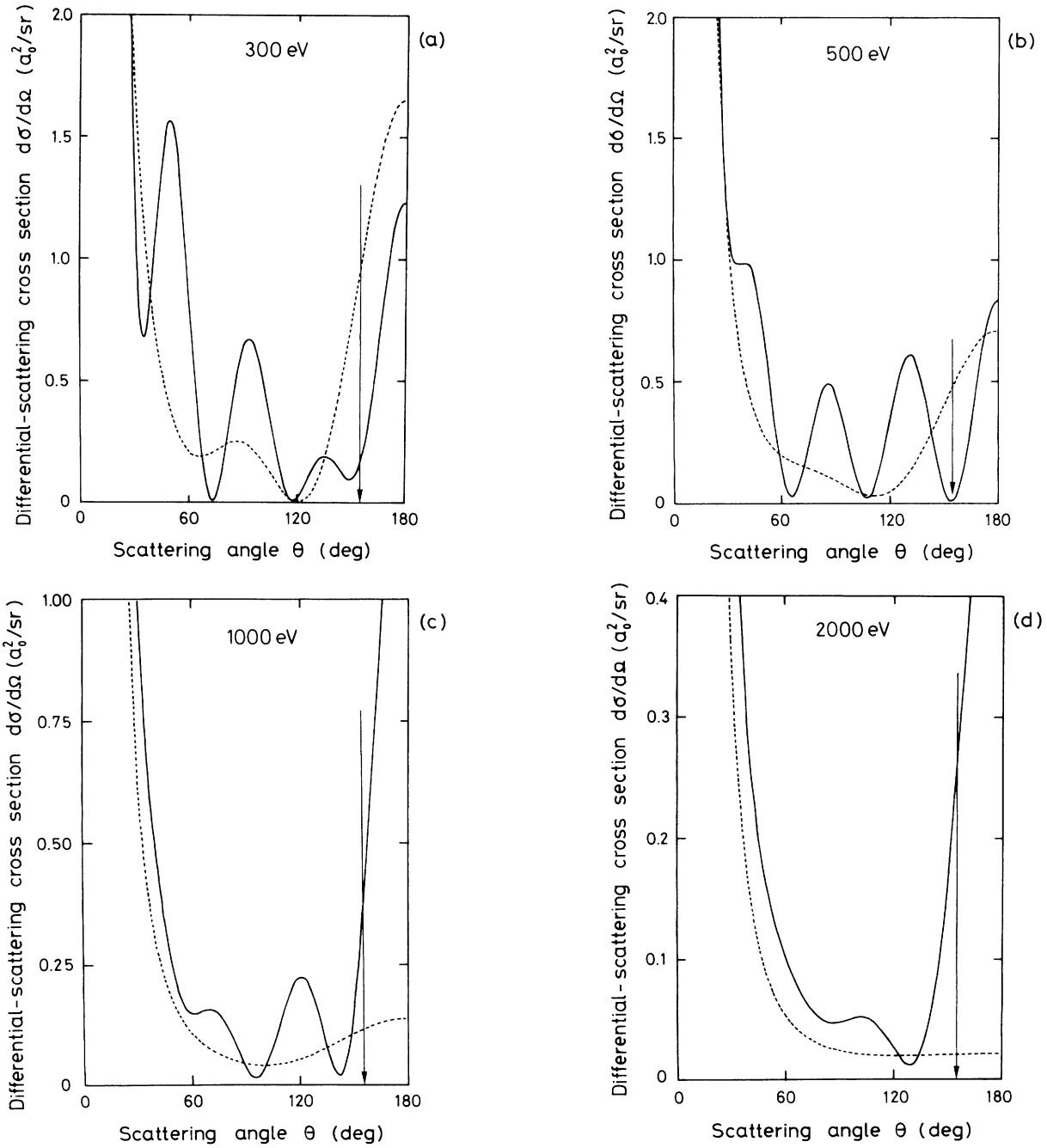

FIG. 3. Angular and energy dependence of the differential-elastic-scattering cross sections calculated within nonrelativistic partial-wave-expansion method. Solid line, gold; dashed line, nickel. Arrows indicate the scattering angle which corresponds to the experimental geometry, i.e., the angle between the electron beam and analyzer axis. (a) 300 eV, (b) 500 eV, (c) 1000 eV, and (d) 2000 eV.

TABLE I. Values of the ratios of the elastic peak intensity measured for the Au/Ni(111) system to the intensity measured for the uncovered nickel surface. These ratios are obtained on dividing the experimental ratios I_E/I_E^{ref} and $I_E^{\text{Ni}}/I_E^{\text{ref}}$.

Au overlayer thickness (Å)	Ratio I_E/I_E^{Ni}			
	300 eV	500 eV	1000 eV	2000 eV
0.0	1.00	1.00	1.00	1.00
2.2	0.629	0.672	1.08	1.45
3.9	0.477	0.495	1.28	1.79
8.4	0.290	0.276	1.32	2.35
14.0	0.224	0.193	1.60	3.38
32.0		0.180	1.75	4.12
44.0	0.198	0.180	1.71	4.18
60.0	0.200/0.209	0.180	1.75	4.28
90.0	0.204	0.174	1.72	4.24

expectations.

The above experiment was simulated with the described Monte Carlo model. Calculations were performed for the same geometry. Only the acceptance angle of the simulated analyzer (cone with half-angle of 10°) was somewhat larger than the acceptance angle of the CLAM analyzer (cone ±6°). At smaller acceptance angles the computer time necessary to reach reasonable accuracy was becoming quite unrealistic. The results of simulations are compared with experimental data in Figs. 2(a)–2(d). Surprisingly, extremely good agreement can be observed. At 300 and 1000 eV, the experimental data are almost reproduced by the theory. Noticeable differences can be seen at 1000 and 2000 eV; however, the trend of the overlayer thickness dependence is predicted correctly. The above unexpected behavior of the gold-on-nickel system can be explained in terms of the relation between *differential*-elastic-scattering cross sections for nickel and gold. Figures 3(a)–3(d) compare the differential-elastic-scattering cross sections at energies considered in the present work. As indicated in the earlier paper,[7] the differential-elastic-scattering cross section for gold has a complicated structure with a number of maxima and minima. The experimental geometry used in the present measurements corresponds to the scattering angle 155°. This angle is indicated with arrow in Figs. 3(a)–3(d). We can see that, indeed, the differential-elastic-scattering cross section for nickel is *larger* than for gold at 300 and 500 eV. This is caused by the fact that the experimental geometry coincides with one of the minima on the differential-elastic-scattering cross sections for gold. This minimum is shifting toward smaller scattering angles with the energy increase, and the relation between differential-elastic-scattering cross sections reverses at sufficiently high energies. Obviously, the differential-elastic-scattering cross sections alone cannot be used for the quantitative description of the elastically backscattered intensities, because of the multiple elastic-scattering collisions. However, they explain very well the origin of the observed effect. Thus we should be aware of the fact that there are certain experimental configurations in which the probability of elastic backscattering from high-atomic-number elements decays dramatically. This effect occurs at different energies for different experimental geometries because of the fact that the position of minima is energy dependent.

An attempt has been made in the present work to visu-

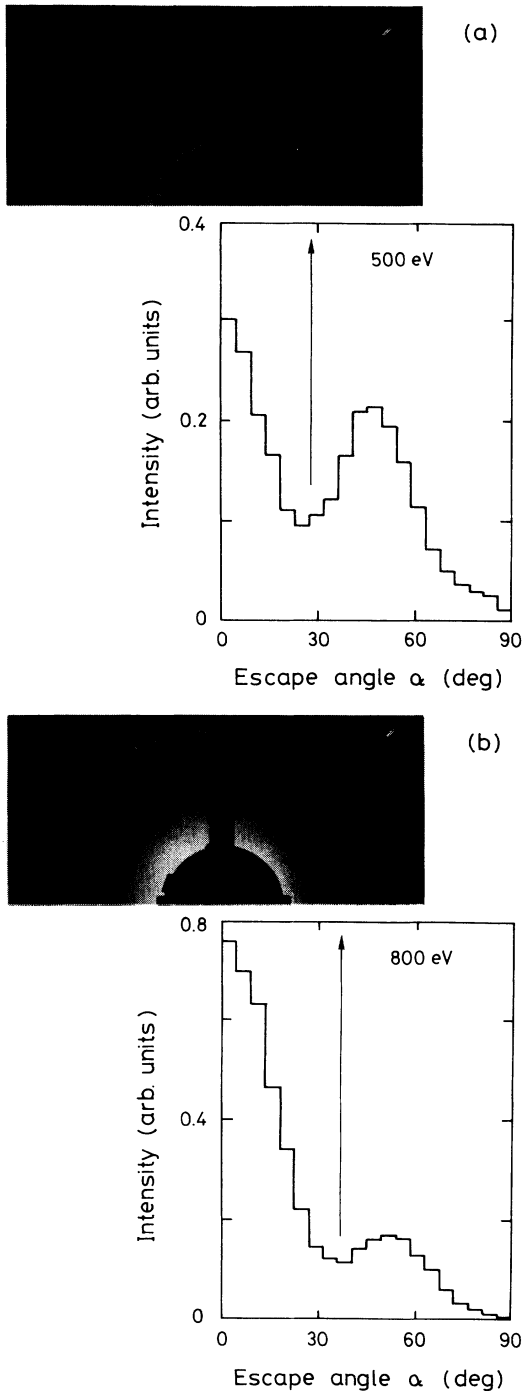

FIG. 4. Comparison of the LEED pattern from the gold sample with an angular distribution of the elastically backscattered electrons predicted by the theory. Both the pattern and histogram have a common angular scale. Note the correspondence in position of the dark ring and calculated minimum. (a) 500 eV and (b) 800 eV.

alize the position of decreased elastic-backscattering probability with the LEED technique. To avoid the crystalline effects, the LEED patterns were recorded for the bulk polycrystalline sample of gold. The patterns obtained at 500 and 800 eV are compared in Figs. 4(a) and 4(b) with the angular distribution of elastically backscattered electrons resulting from the monte Carlo calculations. Indeed, a broad dark ring is observed with position corresponding roughly to the minimum in the calculated distribution. The calculated minimum extends between escape angles 23° and 27° at 500 eV, which coincides with the angle between the analyzer and electron beam in the overlayer experiments. At 800 eV the minimum shifts to the range 36°–40°, which is outside the experimental geometry. Note that the dark zone is slightly more visible at 500 eV than at 800 eV, again in agreement with theory since the minimum in Fig. 4(a) is much more pronounced than the minimum in Fig. 4(b). As follows from Figs. 3(a)–3(d), we can expect that the minimum in the angular distribution continues to shift toward larger escape angles and becomes still less pronounced at energies exceeding 800 eV. The elastic-backscattering effects observed for the gold overlayers are thus mainly due to the energy shift of this minimum.

V. DISCUSSION

As in the case of elemental solids,[6,7] the described theory of elastic backscattering is in good agreement with experimental intensities measured for systems with overlayers. Close inspection of Figs. 2(a)–2(d) reveals two kinds of discrepancies between theory and experiment.

(1) The experimental intensity ratios I_E/I_E^{Ni} observed for small thicknesses of the Au overlayer decrease or increase slightly slower with overlayer thickness as compared with the theoretical ratios. Eventually, the experimental ratios become constant at somewhat higher thicknesses than the theoretical ratios. This effect is observed for all energies.

(2) The experimental ratios I_E/I_E^{Ni} observed for large thicknesses of Au overlayer may differ from the corresponding theoretical ratios (particularly at 500 and 2000 eV).

The first effect may originate from overlayer imperfections. The most obvious explanation ascribes the observed "delay effect" to the formation of an interface of finite thickness. This effect should not be significant. The formation of both liquid and solid Au-Ni alloys is an endothermic process.[22] Thus we can expect that the components have a tendency to separate. Indeed, the phase diagram shows a wide miscibility gap at temperatures below 1000 K.[22] As the gold overlayers were deposited at room temperature, the process of alloying is expected to proceed only to a limited extent.

The discrepancies between theory and experiment at small overlayer thicknesses can be due to other reasons. The Au overlayer thicknesses are known with a rather limited accuracy (about 10–20%). Systematic overestimation of the overlayer thickness would lead to the observed delay effect. This effect can be also argued in terms of the Au island formation. There is some controversy concerning this problem. The XPS analysis in the Au $4f$ feature gives evidence of Au growing according to the model layer by layer,[9] which is in agreement with earlier results.[23] However, similar analysis of the Au $4d$ and Ni $2p$ features does not exclude presence of flat islands on the initial Au layer (layer plus island growth).[10]

In the region of small Au overlayer thicknesses, one can expect serious diffraction effects. At larger thicknesses the LEED pattern becomes diffuse; thus the solid is closer to the model of random distribution of the scattering centers used in calculations. It is rather difficult to estimate quantitatively the contribution to observed deviations arising from the crystallinity of the substrate. Figures 2(a)–2(d) prove that the experimental ratios I_E/I_E^{Ni} measured at large Au thicknesses are in reasonably good agreement with the ratios calculated for the thick overlayer of polycrystalline gold and polycrystalline bulk nickel. If the crystalline effects had a dominant role in the present experimental geometry, the intensity I_E^{Ni} would be considerably affected, leading to dramatic deviation from the theoretical ratio I_E/I_E^{Ni}. Diffraction effects, when present, lead to significant varia-

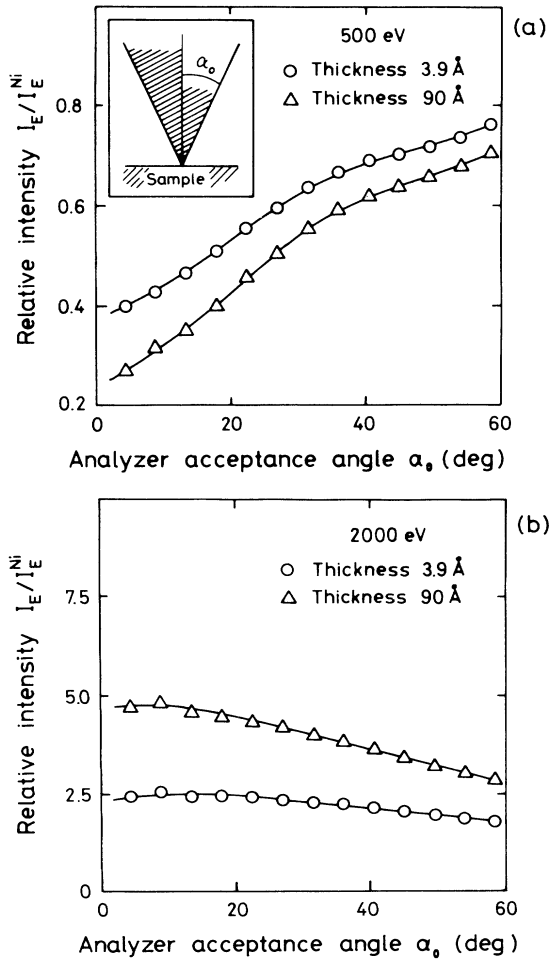

FIG. 5. Dependence of the calculated intensity ratio I_E/I_E^{Ni} on the acceptance angle of the analyzer. Circles, overlayer thickness 3.9 Å; triangles, overlayer thickness 90 Å. (a) 500 eV and (b) 2000 eV.

tions of the electron intensity recorded by a given analyzer. Such a phenomenon was observed by Chang.[24] He has shown that the Auger electron intensity, emitted by the crystalline substrate, changes profoundly with a slight change of the geometry of the measurements. Thus the reasonably good agreement, at all energies, with the theory, neglecting the crystallinity of the sample, is an indication that the role of diffraction is not critical in the present work. This conclusion is supported by earlier observations[6,7] that, generally, the elastic-backscattering theory is rather reliable in the case of polycrystalline elements.

Deviations of the theoretical ratios I_E/I_E^{Ni} observed at large overlayer thicknesses may result for a number of reasons. The simulated geometry involved larger solid acceptance angles than the solid angle of the analyzer. We may expect that the calculated ratio I_E/I_E^{Ni} depends on the acceptance angle α_0, defined in the inset in Fig. 5(a). To check this hypothesis a series of calculations were made for a wide range of acceptance angles. The results are shown in Figs. 5(a) and 5(b). Indeed, we observe a pronounced dependence on the solid angle at energy 500 eV. A decrease of the assumed acceptance angle ($\alpha_0=10°$) to the actual acceptance angle ($\alpha_0=6°$) would then improve the agreement with experiment [Fig. 2(b)], shifting downward the calculated curve by about 20%. On the other hand, the ratios I_E/I_E^{Ni} are practically independent of the acceptance angle at 2000 eV, as shown in Fig. 5(b).

The disagreement between experimental and theoretical intensity ratios may also originate, to a certain extent, from the theory deficiencies. It has been shown that noticeable differences are observed between relativistic and nonrelativistic elastic-scattering cross sections for gold.[6,7] The intensity measured at 25° with respect to the electron beam seems to be slightly overestimated within nonrelativistic calculations.[7] The corresponding relativistic effects for nickel are negligible.[6] Thus application of the relativistic theory in calculations would slightly decrease all the intensity ratios I_E/I_E^{Ni} as compared with the present calculations, although that would involve much more computational difficulties. The accuracy of the theoretical model depends also on the potential approximating the scattering center. The TFD potential is a rather crude approximation of the actual atomic potential. However, it has been shown that, at energies exceeding 200–300 eV, the calculated characteristics of elastically backscattered electrons (angular distribution, backscattering probability, etc.) do not change much if other potentials are used, e.g., the Dirac-Hartree-Fock-Slater potential.[7] The sensitivity of the algorithm to the potential variation decreases with the energy increase.

Finally, one should mention the considerable sensitivity of the calculated intensities to the values of the inelastic mean free path (IMFP) of electrons in a solid.[6] This parameter is usually known with a rather limited accuracy, and because of this fact, one can even reverse the problem. From the elastic-backscattering intensity, which is relatively easy to measure, one can calculate the IMFP.[5] In the present work the values of the IMFP published by Penn[25] and Tanuma, Powell, and Penn[26] were used in calculations. They seem to be most reliable at present. The absolute errors are estimated to be equal to about 10%. These errors may be canceled to a certain extent when calculating the ratios of intensities. Nonetheless, the uncertainties in the values of the IMFP may have the largest impact on the accuracy of the present calculations.

Summarizing, the extension of the elastic-backscattering theory to the systems with overlayers successfully explains the observed intensity variations. The agreement between experiment and theory in the present work is remarkably good, considering all the possible sources of errors. This agreement encourages further efforts to improve the reliability of the theory because of the prospective method for determining the overlayer thickness. Such a method would be very convenient from an experimental point of view, involving only measurements of the elastic peak intensity in the energy spectra. Auger electron spectroscopy[27] and photoelectron spectroscopy[28] were also proposed as potential tools for overlayer thickness measurements. However, these techniques require processing signals of much smaller intensity. Furthermore, the proposed theory of the Auger electron and photoelectron transport is oversimplified, e.g., neglecting the elastic electron collisions in solids.

ACKNOWLEDGMENTS

This work was partially supported by the Danish Natural Science Research Council.

[1]O. A. Baschenko and V. I. Nefedov, J. Electron Spectrosc. **17**, 405 (1979); **21**, 153 (1980); **27**, 109 (1982).

[2]S. Tougaard and P. Sigmund, Phys. Rev. B **25**, 4452 (1982).

[3]A. Jablonski, Surf. Interface Anal. **14**, 659 (1989).

[4]R. Schmid, K. H. Gaukler, and H. Seiler, in *Scanning Electron Microscopy/1983,* edited by O. Johari (SEM, Inc., Chicago, 1983), Vol. II, p. 501.

[5]A. Jablonski, in *Auger Spectroscopy and Electronic Structure,* edited by G. Cubiotti, G. Mondio, and K. Wandelt (Springer-Verlag, Berlin, 1989), p. 186; B. Lesiak, A. Jablonski, Z. Prussak, and P. Mrozek, Surf. Sci. **223**, 213 (1989).

[6]A. Jablonski, J. Gryko, J. Kraaer, and S. Tougaard, Phys. Rev. B **39**, 61 (1989).

[7]A. Jablonski, Phys. Rev. B **43**, 7546 (1991).

[8]M. P. Seah, Surf. Interface Anal. **2**, 222 (1980).

[9]H. S. Hansen and S. Tougaard, Vacuum **41**, 1710 (1990).

[10]H. S. Hansen, C. Jansson, and S. Tougaard, Vac. Sci. Technol. (to be published).

[11]S. Ichimura, M. Aratama, and S. Shimizu, J. Appl. Phys. **51**, 2853 (1980).

[12]R. Shimizu and S. Ichimura, Toyota Foundation Research Report No. I-006, 76-0175, Tokyo, 1981 (unpublished), pp. 8–11.

[13]N. F. Mott and H. S. W. Massey, *The Theory of Atomic Col-*

lisions (Clarendon, Oxford, 1965), pp. 20–24.
[14]F. Salvat, R. Mayol, and J. D. Martinez, J. Phys. B **20**, 6597 (1987).
[15]F. Calogero, *Variable Phase Approach to Potential Scattering* (Academic, New York, 1967), Chap. 3.
[16]L. H. Thomas, J. Chem. Phys. **22**, 1758 (1954).
[17]R. A. Bonham and T. G. Strand, J. Chem. Phys. **39**, 2200 (1963).
[18]F. Salvat and J. Parellada, J. Phys. D **17**, 185 (1984).
[19]D. Liljequist, F. Salvat, R. Mayol, and J. D. Martinez, J. Appl. Phys. **65**, 2431 (1989).
[20]A. Jablonski and S. Tougaard, J. Vac. Sci. Technol. A **8**, 106 (1990).
[21]S. Ichimura and R. Shimizu, Surf. Sci. **112**, 386 (1981).
[22]R. Hultgren, P. D. Desai, D. T. Hawkins, M. Gleiser, and K. K. Kelley, *Selected Values of the Thermodynamic Properties of Binary Alloys* (American Society for Metals, Metals Park, OH, 1973), p. 294.
[23]R. C. Jaclevic, Phys. Rev. B **30**, 5494 (1984).
[24]C. C. Chang, Appl. Phys. Lett. **31**, 304 (1977).
[25]D. R. Penn, Phys. Rev. B **35**, 482 (1987).
[26]S. Tanuma, C. J. Powell, and D. R. Penn, Surf. Interface Anal. **11**, 577 (1988).
[27]P. H. Holloway, J. Vac. Sci. Technol. **12**, 1418 (1975).
[28]M. F. Ebel, G. Zuba, H. Ebel, J. Wernisch, and A. Jablonski, Spectrochim. Acta B **39**, 637 (1984).

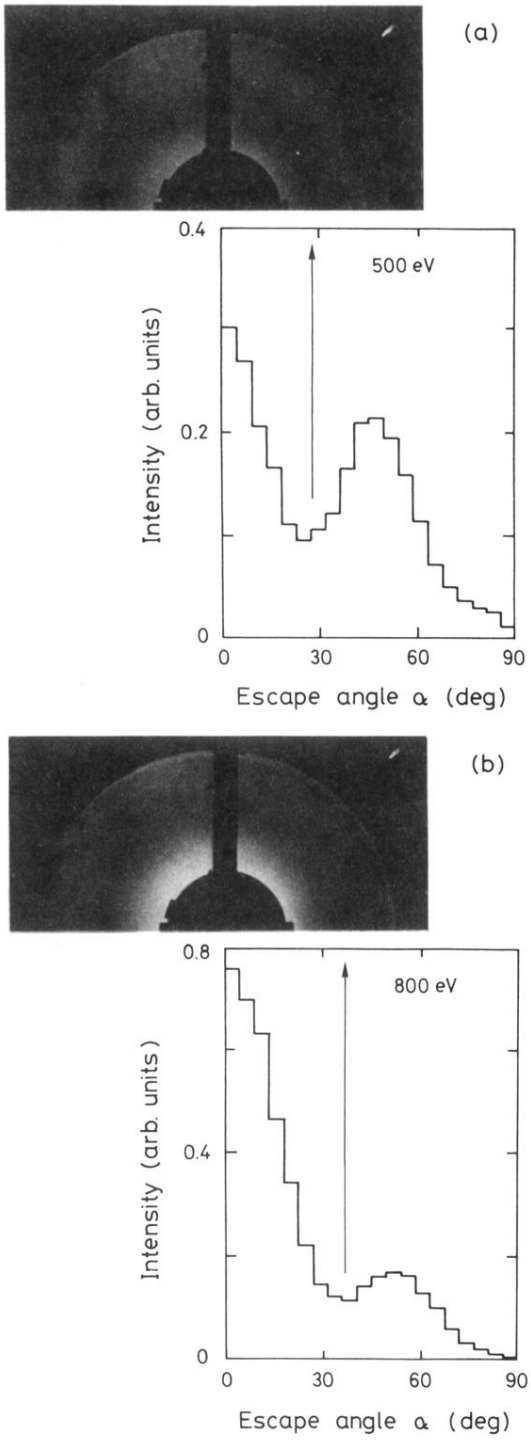

FIG. 4. Comparison of the LEED pattern from the gold sample with an angular distribution of the elastically backscattered electrons predicted by the theory. Both the pattern and histogram have a common angular scale. Note the correspondence in position of the dark ring and calculated minimum. (a) 500 eV and (b) 800 eV.